LEGIBILITY NOTICE

A major purpose of the Technical Information Center is to provide the broadest dissemination possible of information contained in DOE's Research and Development Reports to business, industry, the academic community, and federal, state and local governments.

Altnough a small portion of this report is not reproducible, it is being made available to expedite the availability of information on the research discussed herein.

LA-UR-89-2680

LA-UR--89-2680

DE89 016774

TITLE A Fermi Liquid Electric Structure and the Nature of the Carriers in High-T_c Cuprates: A Photoemission Study

AUTHOR(S) A. J. Arko, R. S List, R. J. Bartlett, S-W. Cheong, Z. Fisk, J. D. Thompson, C. G. Olson, A-B. Yang, R. Liu, C. Gu, B. W. Veal, J. Z. Liu, A. P. Paulikas, K. Vandervoot, H. Claus, J. C. Campuzano, J. E. Schirber, N. D. Shinn

SUBMITTED TO Physica Scripta as the proceedings of the VUV9 Conference in Honolulu, July 17-21, 1989

DISCLAIMER

Los Alamos Los Alamos National Laboratory
Los Alamos, New Mexico 87545

A Fermi Liquid Electronic Structure and the Nature of the Carriers in High-T_c Cuprates: A Photoemission Study

by

A. J.Arko, R. S. List , R. J. Bartlett, S.-W. Cheong, Z. Fisk, J. D. Thompson
Los Alamos National Laboratory, P-10 Group, Los Alamos , NM, 87545

and

C. G. Olson, A.-B. Yang, R. Liu, C. Gu
Ames National Laboratory - USDOE
Iowa State University, Ames, Iowa 50011

and

B. W. Veal, J. Z. Liu, A. P. Paulikas, K. Vandervoort, H. Claus, J. C. Campuzano
Materials Science Division
Argonne National Laboratory, Argonne, IL 60439

and

J. E. Schirber , and N. D. Shinn
Sandia National Laboratories, Albuquerque, NM 87185

Abstract

We have performed angle-integrated and angle-resolved photoemission measurements at 20 K on well-characterized single crystals of high-T_c cuprates (both 1:2:3-type and 2:2:1:2-type) cleaved in situ, and find a relatively large, resolution limited Fermi edge which shows large amplitude variations with photon energy, indicative of band structure final state effects. The lineshapes of the spectra of the 1:2:3 materials as a function of photon energy are well reproduced by band structure predictions, indicating a correct mix of 2p and 3d orbitals in the calculations, while the energy positions of the peaks agree with calculated bands only to within ~0.5 eV. This may yet prove to reflect the effects of Coulomb correlation. We nevertheless conclude that a Fermi liquid approach to conductivity is appropriate. Angle-resolved data, while still incomplete, suggest agreement with the Fermi surface predicted by the LDA calculations. A BCS-like energy gap is observed in the 2:2:1:2 materials, whose magnitude is twice the weak coupling BCS value (i.e., $2\Delta = 7\ KT_c$).

1. Introduction

It is widely accepted that the electronic structure of the high-T_c superconducting (HTSC) cuprates consists of impurity bands induced by the doping of holes into the CuO_2 planes. Many theoretical models [1] assume that the underlying electronic structure is not substantially altered by the doping so that the electronic structure of the HTSCs is similar

to the non-superconducting (or insulating) parent compounds. Since band calculations [2-7], using the local density approximation (LDA), have been singularly unsuccessful in predicting the magnetic and insulating properties of the parent oxides, it is a natural extension to assume that such calculations are inapplicable to HTSCs. The general approaches (aside from band structure) that have been taken include the Anderson model [8,9], some variant of the Hubbard model [10-13] and the resonating valence bond model [14]. To the best of our understanding the last approach results in charge carriers which do not strictly obey Fermi-Dirac statistics so that the system is not described as a Fermi liquid with a well-defined Fermi surface.

Early photoemission measurements, both angle-integrated [15-19] and angle-resolved [20,21] using single crystals, in fact seemed to support the more exotic approaches. While a very small, well-defined Fermi edge was occasionally observed [16] in La-Sr-Cu-O systems, it was never seen in the 1:2:3 type materials [22], thus reinforcing the concept of a vanishingly small density of states (DOS) at E_F and no conventional Fermi function cutoff of normal metals.

The discovery of the Bi-based cuprates with their stable Fermi edge at room temperature changed the above situation and initially actually appeared to be inconsistent with the 1:2:3s and 2:1:4s. We showed [23-26], however, that most early photoemission data on these latter types of compounds, if taken at room temperature, probably were not sampling the true bulk electronic structure but rather only a deteriorated surface oxide (an insulator with no DOS at E_F) resulting from surface reconstruction, oxygen loss, or both (the actual mechanism is yet to be determined). If, however, a well-characterized superconducting single crystal of a 1:2:3 material is cleaved at low temperatures ($T<50K$) to expose a fresh surface, such a surface reconstruction (and/or oxygen loss) is suppressed and a spectrum representative of the bulk superconductor is obtained. This is evidenced by the existence of a large, stable Fermi edge and the appearance of a highly structured photoemission spectrum [27] which, as we shall see, is not inconsistent with a

band structure DOS. Thus a uniformity regarding the Fermi edge is established among the HTSCs (including the BiO_3-based compounds) which now makes them strong candidates for Fermi liquids, as will become evident in the text. Indeed it is now possible to observe directly via photoemission the large BCS-like gap [28-30] at temperatures below T_c, and in fact only for those k-values which correspond to the Fermi surface [29,30].

The weight of evidence is building not only in favor of the Fermi liquid model, but rather also towards an electronic structure in large measure describable by a band structure DOS [27] (at least some form of renormalized bands), and a Fermi surface very similar to predictions. Thus we are apparently not dealing with impurity bands at E_F [31], but rather with bands described by a band calculation. It remains yet to be determined to what extent the bands are renormalized as a consequence of the strong Coulomb correlation which is evidenced in the form of satellites [16,32,33], and whether this correlation plays a significant role in the superconductivity.

In the present manuscript we will review our recent photoemission data which led us to the above conclusions. We will mostly confine ourselves to angle-integrated data since the angle-resolved work is still in progress, although the latter type of data will eventually be much more compelling. We have not studied the parent insulating oxides in any great detail so that we don't know how they differ from the predicted metallic behavior. This latter study is a necessary step in understanding these materials and is at present underway.

2. Experimental Details

A much more detailed set of experimental procedures is published elsewhere [27]. Here we will only concentrate on the essential features.

The angle-integrated photoemission measurements were taken at the Synchrotron Radiation Center in Stoughton, WI using the Ames Montana ERG/SEYA beamline, as well as the Minnesota Argonne-Los Alamos ERG beamline. Overall instrument resolution

for the beamline and the double pass CMA analyzer varied from 125 to 200meV. The chamber pressure was maintained at $5x10^{-11}$ Torr throughout the measurements. Cooling to 20K was accomplished via a closed cycle He refrigerator. The angle-resolved data on the 2:2:1:2s reported here was taken with a VSW 50mm hemispherical analyzer, with a maximum overall resolution (at 2eV pass energy) of 30meV. Chamber pressure was likewise maintained at $5x10^{-11}$ Torr and sample temperature controlled with a He refrigerator.

The thin single crystal plates (typical dimensions 1mm x 1mm x 0.05mm) were mounted with epoxy between two Al rods oriented along the c-axis. Electrical contact was made with a thin layer of a suspended graphite solution. One of the Al rods was in contact with the cold finger while prying *in-situ* on the free Al rod resulted in a sample cleave in the a-b plane.

Most of the measurements reported here were done with the sample temperature maintained at 20K since, as will become evident, warming above 50K resulted in a rapid deterioration of the 1:2:3 surface [23,24]. On the other hand, the sample surface remained stable for up to 2 days if maintained at 20K. A similar instability was not observed for the 2:2:1:2s.

3. Results and Discussion

3.1 Clean vs. Deteriorated Surface of Y-1:2:3 In Fig.1 we show 3 spectra from a $Y:1:2:3{\cdot}O_{6.9}$ crystal cleaved at 20K and measured first at 20K, then at 300K, and again at 20K. A measurement at 20K immediately after a fresh cleave (20_i in Fig. 1) exhibits a large, resolution-limited Fermi edge, and a substantial spectral weight in the -1eV to -2eV range. It does not, however, show the much discussed [34,35] feature at -9eV. If the sample is maintained at 20K the spectrum 20_i can be reproduced indefinitely.

Warming to 300 K, however, immediately results in dramatic changes. Even before the -9eV feature develops significant intensity, the spectrum loses *all* the intensity at

E_F, followed by a substantial loss of intensity in the -1 to -2eV range, a valence band maximum shift from -3.5eV to -4.5eV, and additional intensity loss near -6eV. Cooling the sample back to 20K (spectrum 20_f in Fig. 1) shows that the changes are irreversible, although some apparent recovery is seen near E_F. This recovery is not understood at present but may be related to a phase transition.

It is instructive to follow the behavior of the O-1s core level as the surface deteriorates. In Fig. 2 we show three spectra of this core level. Spectrum (a) is for $Bi_2Sr_2CaCu_2O_8$ after a fresh cleave at 20K, spectrum (b) is for Y:1:2:3 $O_{6.9}$ (same sample as in Fig. 1) likewise after a fresh cleave, while spectrum (c) is for the same sample of Y:1:2:3 but now at 300K. Note that a single O-1s core level is found at -528eV in both materials after a fresh cleave. As the surface of the 1:2:3 material deteriorates, a second O-1s peak at -531eV grows, along with the -9eV peak. Some researchers have assigned [36,37] the -531eV peak to the O^{1-} valence state (vs. the O^{2-} for the -528eV peak). However, we can see that it is not intrinsic to the $O_{6.9}$ material.

The question arises whether the deterioration is due to oxygen loss resulting in an oxygen deficient Y:1:2:3 surface, or to a chemical change [38] resulting in a totally different composition at the surface. We can get some insight by studying well-characterized oxygen-deficient crystals cleaved and measured under identical conditions as the $O_{6.9}$ sample. The spectra for several $YBa_2Cu_3O_x$ materials are shown in Fig. 3 at hν=50eV. We can see that while the DOS at E_F decreases monotonically with x, there is no indication of the -9eV peak in any spectrum, and the valence band maximum remains at -3.5eV for all x. There is, however, a significant narrowing of the valence band width for x=6.25, with significant accompanying intensity losses at -1.5eV.

We conclude from Fig. 3 that while decreasing the oxygen content does indeed cause some changes throughout the valence bands, a spectrum taken at room temperature on a deteriorated surface is totally unrelated to that of a 1:2:3 material. Perhaps some oxygen loss is occurring. However, a more significant factor for UV photoemission

measurements with their small escape depths is a composition change [38] on the surface which yields the -9eV feature in the valence bands, as well as the -531 eV peaks in the O-1s spectrum. Thus attempts to correlate these features with valence fluctuations or other phenomena intrinsic to the 1:2:3 materials, are in error.

3.2 Valence Bands of Y:1:2:3; Comparison to Band Calculations Having established the instability of the 1:2:3 surface at elevated temperatures, it is clear that meaningful data can only be obtained on a freshly-cleaved single crystal surface at T<50K. The bulk of the remaining data was taken under such conditions.

In Fig. 4 we display a series of angle integrated spectra from a sample of $YBa_2Cu_3O_{6.9}$ taken at various photon energies ranging from 14eV to 70eV. We point out that these spectra are from a sample different from that of Fig. 1. This caution is necessary since it is evident that at hν=50eV the spectra from the two samples are not identical. The differences are due to residual angle resolved effects stemming from the fact that we are using single crystals and a CMA analyzer which admits only a limited number of electron trajectories. Hence we do not have a true angle integrated spectrum. These phenomena would however tend to affect amplitudes more than peak positions in these very complex materials so that it does not alter our conclusions. We wish to call attention to the following observations:

(a) At low hν (<20eV) we observe a number of peaks in the secondary electron spectrum due to van Hove singularities in the empty bands [39]. These peaks shift linearly with photon energy to apparent higher binding energies as hν increases, as shown by the arrows for one set of such final state peaks. They are not representative of the filled states except insofar as they will enhance a valence band feature whenever direct transitions are possible into these van Hove singularities from the filled states. Thus most of the apparent dispersion for hν<20eV is due to these final state effects.

(b) In addition to the peak at E_F, we can identify peaks A through F as being part of the DOS structure.

(c) The Fermi edge amplitude is strongly modulated by the same band structure effects as in (a), but remains strong for all hν, thus indicating at least a partial d-wave function character (see below).

When one compares the peaks in the spectra to a calculated [2-7] DOS (Fig. 5) it is possible to get a one-to-one correspondence between the calculated and experimentally observed peaks, provided that the calculated Fermi energy is shifted up (to lower binding energies) by 0.5eV. We show in Fig. 5 a DOS from Ref. , although most calculated band structures are similar. Peaks A and B are primarily due to p-like bands while the bulk of the Cu-3d density is centered around peaks C and D. The weak peak F is due to the bottom of the oxygen-p bonding bands.

The actual character of peaks A through F can be more easily discerned form the lineshapes of the spectra as a function of photon energy. Because of the very different cross sections [40] for p vs. d transitions, the spectral weight changes as hν increases. Redinger *et. al.* [41] have calculated the expected photoemission spectra as a function of hν based on their DOS. We compare several of the spectra of Fig. 4 to these predicted spectra in Fig. 6. The solid curves are spectra from Fig.4 with backgrounds subtracted, while the dashed curves are from Ref. 41. The spectra were aligned on the p-like peak A. Except for the 0.5eV shift we see that the spectral shape follows the correct energy dependence, thus indicating a correct orbital character mix in the DOS. On this gross scale, then, band calculations correctly capture the essential feature of the experimental DOS. The main disagreement is the 0.5eV shift and the very large predicted Fermi edge (large $N(E_F)$) vs. a much more modest one observed experimentally.

A very recent publication [42] has focused on the problem of Coulomb correlation and how it should affect the band structure as obtained from an LDA calculation. Indeed, they find that for a value of U~4.0eV, the Fermi energy would shift

by ≈0.5eV with a corresponding dramatic drop in $N(E_F)$, just as observed. This fact, combined with the obvious satellite structure associated with Cu features, would seem to support a band structure at least partially renormalized by Coulomb correlation, a situation somewhat reminiscent of heavy Fermions.

3.3 The Character of States at E_F It is quite important to a number of theories [1] to determine the orbital character of the states at E_F. For example, many theories would prefer primarily O-2p character with oxygen hole hopping in the CuO_2 planes as the primary conduction mechanism. While resonant photoemission has been the technique of choice [43] for determining orbital symmetry of photoemission features, a quick glance at Fig. 7 will show that this technique has its shortcomings with respect to HTSC's. Here we show spectra from a slightly deteriorated sample of Eu:1:2:3 at both the O-2s (left panel) and Cu-3p (right panel) edges. We do this in order to focus on the -9eV contamination peak, which is known to be of primarily O-2p character. We see that it has a maximum amplitude at hν=22eV, as does the valence band feature at -2eV below E_F, which we know from above to also be substantially p-like in character. Thus we conclude that at least for 1:2:3 type materials, the oxygen resonance is at hν=22eV and not at the often quoted [31] 18 eV. The intensity at E_F, on the other hand, has minimum at hν=22eV. The Fano resonance, if any, is obscured by the above-mentioned final state effects (van Hove singularities in the empty state) due to band structure.

Similarly at the 3p edge (hν=74eV) one runs into difficulties. Note that there is almost no intensity modulation in the valence bands, while the -10eV and -12eV Cu satellites (arrows) undergo a very strong resonance. The point is that even if there is 3d character at E_F there is no reason to expect its intensity to resonate at hν=74eV since the entire valence band fails to resonate.

One can still determine the orbital character by measuring the intensity at E_F as a function of photon energy. In Fig. 8 we display angle integrated spectra of $Bi_2Sr_2CaCu_2O_8$ for a number of photon energies normalized at the valence band

maximum. While this is an incorrect normalization procedure one nevertheless sees that the intensity of the peak near E_F (actually at -0.2eV) remains strong to high photon energies, and shows final state enhancements at 18eV and 50eV.

A more correct normalization takes into account the number of p-and d-electrons (we ignore all the rest due to weak cross-sections [40]) and equates the total integrated intensity of the spectrum at each photon energy to the total integrated intensity expected at that energy from the atomic calculations of Yeh and Lindau [40]. The resulting intensity at -0.2eV is then plotted as a function of hν in Fig. 9. Here the open circles correspond to values of hν where final state enhancements occur and hence are not included in the calculations. The solid lines are intensity variations expected of the feature were either entirely d-like or p-like. Clearly the measured intensity follows neither curve. Instead we try to approximate it by taking linear combinations of the two cross-sections and find a best fit with ≈35% Cu-3d and 65% O-2p character. Similar analyses for the 1:2:3 material yield about a 20-80 mix of Cu and O at E_F.

It is difficult to put error bars on these numbers since, as we have seen, the intensity, especially at E_F, is a strong function of the sample surface condition, as well as sample orientation (recall that our measurements are not truly angle integrated). Suffice it to say that there are strong contributions from both Cu and O in the conduction band. This, then, also argues in favor of a strongly-hybridized band-like model.

3.4 Angle-Dispersive Bands and the BCS-Like Energy Gap

Angle resolved photoemission may in the end prove to be the most significant measurement with which to probe the electronic structure of HTSCs, and a substantial amount of angle-resolved data already exists in literature [31,44,45]. We would caution the reader, however, to be cognizant of the very serious sample-dependence encountered. We would automatically discard, for example, any room temperature data on the 1:2:3 samples even though a weak Fermi edge may be evident (refer to Fig. 1). Likewise we are wary of data which features the -9eV satellite. In the case of the 2:2:1:2 materials we would point out that the Fermi edge in our samples (Fig. 8) is much stronger than in most other published data [31,45], presumably reflecting sample perfection. On top of all this are the very strong final state modulation effects which greatly increase the parameter space in which to map out the bands. In other words, the absence of a peak in the spectrum does not automatically translate into the absence of a band. It may be missing because of a weak matrix element (i.e., no final state exists for direct transitions at that hν).

Most published angle-resolved data [31] were taken at hν=18eV, because it is generally believed that a resonant enhancement occurs there. We, however, would not rule out the possibility that for hν=18eV one merely enhances one part of the Brillouin zone due to final state effects, so that a failure to work at other values of hν precludes a proper sampling of other parts of the zone. In addition, strong polarization effects have been observed suggesting that one should not rely too heavily on symmetry.

Our own angle resolved work is still in progress, with indications that this will be a long project, indeed. We are not prepared to make definitive statements at this time. However, preliminary indications are that the Fermi surfaces predicted both for the 1:2:3-type and the 2:2:1:2-type materials will be borne out experimentally. The bands themselves, however, are difficult to follow below ≈300meV in $Bi_2Sr_2CaCu_2O_8$ so that we cannot make definitive statements about band-widths. We do, however, find less disagreement in general with calculated bands than others have observed.

In this manuscript we will confine ourselves to the more definitive aspects of the

data. In Fig. 10 we show a series of spectra taken on $Bi_2Sr_2CaCu_2O_8$ at the indicated angles with respect to the c-axis at hν=22eV. For this set of data, $k_{||}$ is approximately along the Γ-M direction. Two sets of data are shown for each angle setting of the analyzer (2° acceptance angle); thin lines correspond to spectra obtained at T=90K (i.e., at $T>T_c=85$), while the thicker lines correspond to data taken at $T=20K<<T_c$. It will be noticed that for an analyzer setting of Θ=11° the peak maximum in the spectrum is at -100 meV, well below E_F, and easily resolvable with our overall instrument resolution of 30meV. In short, the band is still below the Fermi energy and not involved in conduction. At Θ=18°, however, the band disperses much closer to E_F and the 90K spectra are vastly different from the 20K spectra. This is the effect of the BCS-like gap, Δ, at E_F and the associated pile-up of states just below Δ.

Before discussing the effect of the gap in more detail, let us first concentrate on the 90K spectra. for Θ=18° there is a clear indication of the band crossing E_F as evidenced by the dramatic drop in intensity. Because the above data were not taken precisely along a symmetry axis, there is no direct band calculation for comparison. Nevertheless the crossing is approximately in the location where one would expect the M-centered Fermi surface. Data presently presently being analyzed on better oriented samples appear to indicate nearly exact agreement with the predicted Fermi surface [46].

Because of our 2° acceptance cone of photoemitted electrons, each spectrum in Fig. 10 is simultaneously sampling approximately ≈10% of the Γ–M momenta (≈ 0.075 $Å^{-1}$). However, for Θ=18°, most of the band being sampled has dispersed above E_F and we can get there a much more accurate measure of the sharpness of the Fermi edge and how it compares to what one expects from a conventional metal. Using the usual 10% to 90% of peak height to determine the width of the Fermi edge, we obtain a value of ≈45meV. Using the same criteria for the Fermi function broadening, the Fermi edge at T=90K is expected to be broadened by ≈35meV (note that kT≈8meV at this temperature) while instrument broadening is ≈30meV. The rms value of these two broadenings is

46meV which is almost exactly our observed value. Thus we have an electronic structure which obeys Fermi-Dirac statistics–in short, a Fermi liquid!

Returning to the 20K spectra we note the pile-up of states which results in the sharp peaks (FWHM=30meV, or, the instrument resolution) just below the gap, Δ. To determine Δ we modeled [30] the Θ=18° spectrum with a Lorentzian and a linear term (because of the finite angular acceptance of the analyzer this was again deemed the least complicated spectrum). The width of the 90K Lorentzian was determined empirically (presumably a function of lifetime broadening and dispersion of initial and final state bands). This was then convolved with a 90K Fermi function and instrument broadening to obtain a best fit. Finally the "best fit" Lorentzian was convolved with a BCS density of states function [47] and a 20K Fermi function. In this way a best fit to the data at 20K was obtained for $2\Delta=7kT_c$. This is similar to values previously reported [28,29], although our data are much more free of complications resulting from angle integration. A cursory measurement of the amplitude of the BCS density of states (i. e., a simple scaling of excess peak height vs. temperature) indicates that the pile-up of states with temperature roughly follows a Brillouin function.

The very large gap (twice the BCS weak coupling value) may be indicative of strong coupling effects in accordance with the results of Kresin [48], who has shown that the limiting value for extremely strong coupling is $8kT_c$. Indeed we have additional evidence from the variation of $N(E_F)$ with T_c that strong coupling effects may be indicated. In Fig. 3 we see that $N(E_F)$ (actually we use the maximum value of the spectral density just below E_F) drops very rapidly with T_c. Kresin in fact has shown from the generalized Eliashberg equations that in the generalized case for any value of the coupling constant, λ,

$$T_c=0.5\langle\omega^2\rangle^{1/2}(e^{2/\lambda}-1)^{-1/2}$$

where the prefactor $A=0.5\langle\omega^2\rangle^{1/2}$, is related to the Debye temperature and is allowed to vary to obtain the necessary T_c. If we make the assumption that, as in the BCS

formulation, $\lambda=N(E_F)V$, where V is a constant interaction strength, then λ is proportional to $N(E_F)$. In Fig. 11 we plot a series of curves for the function

$$T_c=A(e^{2\lambda_{max}/\lambda}-1)^{-1/2},$$

where A and λ_{max} for each curve are adjusted so that T_c=92K at $\lambda=\lambda_{max}$. In the limiting case of large λ_{max} we have $T_c=92(\lambda/\lambda_{max})^{1/2}$ or, equivalently,

$$T_c=92[N(E_F)/N(E_F)_{max}]^{1/2}.$$

Here $N(E_F)_{max}$ is the value of $N(E_F)$ for the Tc=92K material. We can see from the figure that, while the error bars are large, T_c varies approximately as $[N(E_F)]^{1/2}$, or the strong coupling limit.

4. Conclusions

We believe that there is ample indication that band structure calculations have captured the essential features of the DOS in HTSC materials. While some renormalization of the bands due to electron-electron correlation effects may still prove necessary, the indications are that we are dealing with a conventional Fermi liquid whose Fermi surface is adequately described by LDA calculations. A BCS-like energy gap is observed in the 2:2:1:2 materials whose value is about twice the weak-coupling BCS value, but the density of states just below Δ is correctly described by the BCS function. The large gap and the rapid variation of $N(E_F)$ with T_c would seem to support a strong coupling model. Previous inconsistencies in photoemission data are primarily due to the use of sintered materials and measurements at room temperature which yield a surface composition different from the bulk.

Acknowledgements

This work was performed under the auspices of the U.S. Department of Energy. The Ames Lab. acknowledges DOE support under contract # W-7405-ENG82 while Argonne National Lab acknowledges DOE support under contract # W-31-109-ENG-38. The Synchrotron Radiation Center, whose staff we wish to gratefully acknowledge for their assistance, is supported by the NSF under contract #DMR8601349. We wish to

acknowledge illuminating discussions with S. Trugman, B. Brandow, F. M. Mueller, and R. L. Martin.

References

1. For a compilation of the various approaches see, "**Theories of High Temperature Superconductivity**," ed. by J. Woods Halley, (Addison-Wesley) 1988.

2. For a complete list of references on various band structure calculations, see the review article by Warren E. Picket, to be publisehd in Rev. Mod. Phys.

3. J. Yu, A. J. Freeman, and J. H. Xu, Phys. Rev. Lett. **58**, 1035 (1987). S. Massida, J. Yu, and A. J. Freeman, Phys. Rev. B **38**, 11352 (1988); J. Yu, A. J. Freeman, and S. Massida, "**Novel Superconductivity**", eds. S. A. Wolf and V. Z. Kresin, (Plenum, New York, 1987) p. 367.

4. L. F. Mattheiss and D. R. Hamann, Phys. Rev. Lett. **60**, 2031 (1988).

5. F. Herman, R. V. Kasowski, and W. Y. Hsu, Phys. Rev. B **38**, 204 (1988); W. Y. Hus and R. V. Kasowski, "**Novel Superconductivity**" , eds. S. A. Wolf and V. Z. Kresin (Plenum, New York, 1987) p. 373.

6. W. Y. Ching, Yongnian Xu, Guang-Lin Zhao, K. W. Wong, and F. Zandiehnadem, Phys. Rev. Lett. **59**, 1333 (1987).

7. B. Szpunar, V. H. Smith, and R. W. Smith, Physica **C152**, 91 (1988); W. M. Temmerman, Z. Szotek, and G. Y. Guo, J. Phys. **C21**, L867 (1988).

8. A. Fujimori and F. Minami, Phys. Rev. **B30**, 957 (1984) A. Fujimori, M. Saeki, N. Kimizuka, M. Taniguchi, and S. Suga, Phys. Rev. **B34**, 7318 (1987); A. Fujimori, in "Strong Correlation and Superconductivity," eds. H. Fukuyama, S. Maekawa, and A.P. Malozemoff (Springer, Berlin, 1989) pp. 1-12.

9. G. van der Laan, C. Westra, C. Haas, and G.A. Sawatsky, Phys. Rev. **B23**, 4369 (1981); G.A. Sawatsky and J.W. Allen, Phys. Rev. Lett. **53**, 2339 (1985); J. Zaanen, G.A. Sawatsky, and J.W. Allen, Phys. Rev. Lett. **55** 8060 (1986).

10. V. Emery, Phys. Rev. Lett. **58**, 1196 (1987).

11. F.C. Zhang and T.M. Rice, Phys. Rev. **B37**, 3759 (1988).

12. C.M. Varma, S. Schmitt Rink and E. Abrahams, Sol. St. Comm. **62**, 681 (1987).

13. J.E. Hirsh, Phys. Rev. **B35**, 8726 (1987).

14. P.W. Anderson, Science **235**, 1196 (1987); P.W. Anderson, G. Baskaran, Z. Zou and T. Hsu, Phys. Rev. Lett. **58**, 2790 (1987).

15. G. Wendin, J. Phys. (Paris) Colloq. **48**, C9-483 (1987); G. Wendin, Physica Scripta, (1989).

16. Z. X. Shen, J. W. Allen, J. J. Yeh, J S. Kang, W. P. Ellis, W. E. Spicer, I. Lindau, M. B. Maple, Y. D. Dalichauch, M. S. Torikachlivi, J. Z. Sun, and T. H. Geballe, Phys. Rev. B **36**, 8414 (19).

17. P. Steiner, J. Albers, V. Kinsinger, I. Sander, B. Siegwort, S. Huffner, and C. Politis, Z. Phys. B, **66**, 275 (1986); P. Steiner, V. Kinsinger, I. Sander, B. Siegwart, S. Huffner, and C. Politis, Z. Phys. B **67**, 19 (1987).

18. P. D. Johnson, S. L. Qui, L. Jiang, M. W. Ruckman, M. Strongin, S. L. Hulbert, R. F. Garrett, B. Sinkovic, N. V. Smith, R. J. Cava, C. S. Lee, D. Nichols, E. Koczanowicz, R. E. Salomon, and J. E. Crow, Phys. Rev. B **35**, 8811 (1987).

19. J. H. Weaver, H. M. Meyer III, T. J. Wagener, D. M. Hill, Y. Gao, D. Peterson, Z. Fisk, and A. J. Arko, Phys. Rev. B **38**, 4668 (1988).

20. N. G. Stoffel, Y. Chang, M. K. Kelly, L. Dottl, M. Onellion, P. A. Morris and W. A. Bonner, Phys. Rev. B **37**, 7952 (1988); Ming Tang, N. G. Stoffel, Qi Biao Chen, D. La Graffe, P. A. Morris, W. A. Bonner, G. Margaritondo, and M. Onellion, Phys. Rev. B **38**, 897 (1988).

21. M. Onellion, Ming Tang, Y. Chang, G. Margaritondo, J. M. Tarascon, P. A. Morris, W. A. Bonner, and N. G. Stoffel, Phys. Rev. B **38**, 881 (1988).

22. A weak irreproducible Fermi edge was reported by G. Rossi, A. Revcolevschi, and J. Jegoudes, Int. J. Mod. Phys. B **1**, 831 (1987).

23. A. J. Arko, R. S. List, Z. Fisk, S-W. Cheong, J. D. Thompson, J. A. O'Rourke, C. G. Olson, A-B. Yang, T-W. Pi, J. E. Schirber, and N. D. Shinn, J. Mag. Mag. Mater. Lett. **75**, L1 (1988).

24. R. S. List, A. J. Arko, Z. Fisk, J. D. Thompson, C. B. Pierce, D. E. Peterson, R. J. Bartlett, N. D. Shinn, J. E. Schirber, B. W. Veal, A. P. Paulikas, and J. C. Campuzano, Phys. Rev. B **38** (Rapid Comm.) , 11966 (1988).

25. R. S. List, A. J. Arko, Z. Fisk, S-W. Cheong, S. D. Conradson, J. D. Yhompson, C. B. Pierce, D. E. Peterson, R. J. Bartlett, J. A. O'Rourke, N. D. Shinn, J. E. Schirber, C. G. Olson, A-B. Yang, T-W. Pi, B. W. Veal, A. P. Paulikas, and J. C. Campuzano, to be published in the Proceedings of the American Vacuum Society Conference, Atlanta, Oct. 3. 1988.

26. R. S. List, A. J. Arko, Z. Fisk, S-W. Cheong, J. D. Thompson, J. A. O'Rourke, C. G. Olson, A-B. Yang, T-W. Pi, J. E. Schirber, and N. D. Shinn, Submitted to J. Appl. Phys.

27. A.J. Arko, R.S. List, R.J. Bartlett, S-W. Cheong, Z. Fisk, J.D. Thompson, C.G. Olson, A-B. Yang, R Liu, C. Gu, B.W. Veal, J.Z. Liu, A.P. Paulikas, K. Vandervoort, H. Claus, J.C. Campuzano, J.E. Schirber, and N.D. Shinn, Phys. Rev. **B40**, [in Press].

28. J.-M. Imer, F. Patthey, B. Dardel, W.-D. Schneider, Y. Baer, Y. Petroff, and A. Zettl, Phys. Rev. Lett., **62**, 336 (1989).

29. R. Manzke, T. Buslaps, R. Claessen, and J. Fink, Europhysics Lett., [in Press].

30. C.G. Olson, R. Liu, A-B. Yang, D.W. Lynch, A.J. Arko, R.S. List, B.W. Veal, Y.C. Chang, P.Z. Jiang, and A.P. Paulikas, Science [in Press].

31. T. Takahashi, H. Matsuyama, H. Katayama-Yoshida, Y. Okabe, S. Hosoya, K. Seki, H. Fujimoto, M. Sato, and H. Inokuchi, Nature **334**, 691 (1988); T. Takahashi, H. Matsuyama, H. Katayama-Yoshida, Y. Okabe, S. Hosoya, K. Seki, H. Fujimoto, M. Sato, and H. Inokuchi, Phys. Rev. B (to be published).

32. D. D. Sarma, Phys. Rev. B **37**, 7948 (1988).

33. J. Zaanen, G. A. Sawatsky, and J. A. Allen, Phys. Rev. Lett. **55**, 418 (1985).

34. W. K. Ford, C. T. Chen, J. Anderson, J. Kwo, S. H. Liou, M. Hong, G. V. Rubenacker and J. E. Drumheller, Phys. Rev. B **37**, 7924 (1988).

35. N. G. Stoffel, P. A. Morris, W. A. Bonner, D. LaGraffe, Ming Tang, Y. Chang, G. Margaritondo, and M. Onellion, Phys. Rev. B **38**, 213 (1988).

36. D. van der Marel, J. van Elp,G.A.Sawatsky,andD.Heitman,Phys. Rev. B37, 5136(1988).

37. T. Gorieoux, G. Krill, M. Maurer, M. F. Ravet, A. Menny, H. Tolentino, and A. Fontaine, Phys. Rev. B37, 7516 (1988).

38. T. Takahashi, F. Maeda, H. Katayama-Yoshida, Y. Okabe, T. Suzuki, A. Fujimari, S. Hosoya, S. Shamoto, and M. Sato, Phys. Rev. **B37**, 9788 (1988).

39. F. J. Himpsel, Applied Optics, **19** ,3964 (1980).

40. J. J. Yeh and I. Lindau, Atomic Data and Nuclear Data Tables **32**, 1 (1985).

41. J. Redinger, A. J. Freeman, J. Yu, and S. Massida, Phys. Lett. **A124**, 469 (1987).

42. J. Costa-Quintana, F. Lopes-Aguilar, S. Balle, and R. Salvador. Phys. Rev. **B39**, 9675 (1989).

43. U. Fano, Phys. Rev. **124**, 1886 (1961).

44. Y. Sakisaka, T. Komeda, T. Maruyama, M. Onchi, H. Kato, Y. Aiura, H. Yanashima, T. Terashima, Y. Bando, K. Iijima, K. Yamamoto, and K. Hirata, Phys. Rev. **B39**, 2304 (1989); and Phys. Rev. **B39**, 9080 (1989).

45. F. Minami, T. Kimura and S. Tackawa, Phys.Rev. **B39**, 4788 (1989).

46. S. Massida, J. Yu and A.J. Freeman, **C52**, 251 (1988).

47. Y. Chang, Ming Tang, R. Zanoni, M. Onellion, R. Joynt, D.S. Huber, G. Margaritondo, P.A. Morris, W.A. Bonner, J.M. Tarascon, and N.G. Stoffel, Phys. Rev. **B39**, 4740 (1989).

48. V. Z. Kresin, Phys. Lett A **122**, 434 (1987).

49. B. W. Veal, C. G. Olson, A. J. Arko, R. S. List, R. Liu, A.-B. Yang, C. Gu, R. J.Bartlett, J. Z. Liu, K. Vandervoort, A. P. Paulikas, and J. C. Campuzano, Physica C **158,** 276 (1989).

Figure Captions

Fig. 1 Valence band spectra for a crystal of $YBa_2Cu_3O_{6.9}$ in the a-b plane. Sample was cleaved at 20K. Lowest curve, 20i, was taken immediately after the cleave, the middle curve was taken within 10 min. of warming to 300K, while the top curve was again taken at 20K upon re-cooling. Note the irreversibility of the various spectral changes (see Text).

Fig. 2 O-1s core level spectra showing the single line nature of the clean spectra; a) $Bi_2Sr_2CaCu_2O_8$ at 20K after a fresh cleave; b) $YBa_2Cu_3O_{6.9}$ at 20K after a fresh cleave; c) $YBa_2Cu_3O_{6.9}$ after ≈1/2 hr at 300K. Note the buildup of a feature at -531eV as the surface deteriorates.

Fig. 3 Valence band spectra for $YBa_2Cu_3O_x$ at hν=50eV for values of x between 6.25 and 6.9, taken on crystals cleaved and measured at 20K. The -9eV satellite is absent for all values of x. Note the decrease in $N(E_F)$ as x decreases. Note also that the valence band maximum is at ≈-3.5eV for all x.

Fig. 4 Angle-integrated valence band spectral for $YBa_2Cu_3O_{6.9}$ for values of hν ranging from 14 to 70eV. The apparent dispersion below hν ≈20eV is due to van Hove singularities in the empty states (see Text). The amplitude modulation of the Fermi edge with hn is due to the same phenomenon. Peaks A through F can be identified with the DOS.

Fig. 5 Density of States taken from Ref. 6. The peaks labelled A through F has a one-to-one correspondence with peaks A through F in Fig. 4 if the calculated Fermi energy is shifted by 0.5eV to lower binding energy.

Fig. 6 Comparison of calculated and measured photoelectron spectra. Solid lines are spectra taken from Fig. 4 but with the secondary background subtracted. Dashed lines are calculated spectra from Ref. 41. Good correspondence is again obtained if we employ the 0.5eV shift.

Fig. 7 Spectra taken on a slightly deteriorated sample of $EuBa_2Cu_3O_{6.9}$ in order to see the resonance of the -9eV contamination peak. Left panel: O-2s feature at -2eV. An incidental Eu-4f resonance at -5eV for a photon energy of hν=18eV is also observed. Right panel: Cu-3p absorption edge. A large resonant enhancement is observed in the -10eV and -12eV Cu-related satellites, while almost no enhancement is seen in the valence bands.

Fig. 8 Valence band spectra for $Bi_2Sr_2CaCu_2O_8$ at T=20K for various values of hν. The intensity of E_F is nearly constant for all spectra except for the final state enhancements at 18eV and 50eV.

Fig. 9 Plot of the photoemission cross-section at E_F for $Bi_2Sr_2CaCu_2O_8$ for properly normalized spectra (see Text) for values of hν ranging form 18eV to 100eV. Open circles represent final state enhancements and are not modeled in the fit. The pure Cu-3d and O-2p cross-sections shown for comparison are taken from Ref. 40. The measured cross-section can be obtained from a linear combination of 35% Cu-3d and 65% O-2p.

Fig. 10 Angle-resolved valence band spectra within 300meV of E_F for $Bi_2Sr_2CaCu_3O_8$ at $h\nu$=22eV. Thin lines are data taken at 90K (above T_c=85K), and thick lines are data taken at 20K. The indicated angles, Θ, are with respect to the c-axis and approximately along the Γ-M direction. Note the pile-up of BCS states for the T=20K data for $\Theta \geq 13^\circ$; *i.e.*, for occupied bands within Δ of E_F.

Fig. 11 Plot of the intensity at E_F from Fig. 3 (data points) as a function of T_c. Note the approximate $[N(E_F)]^{1/2}$ variation. Solid lines are plots of the equation $T_c = A(e^{-2\lambda max/\lambda} - 1)^{1/2}$ for the indicated values of λ_{max}. The prefactor A is adjusted so that T_c=92K for each λ_{max}.

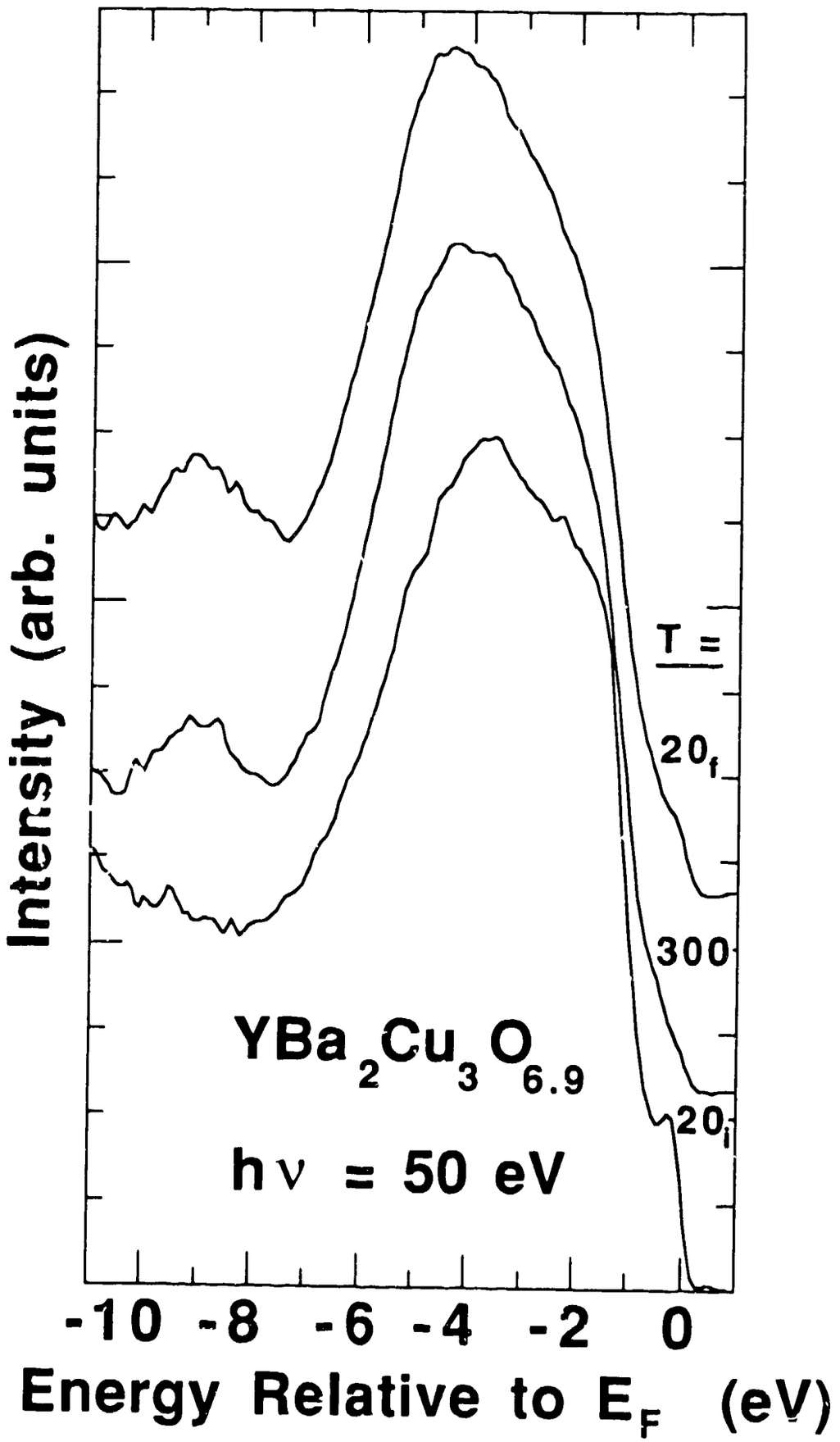
Intensity (arb. units)
T =
20f
300
20i
YBa2Cu3O6.9
hν = 50 eV
-10
-8
-6
-4
-2
0
Energy Relative to EF (eV)

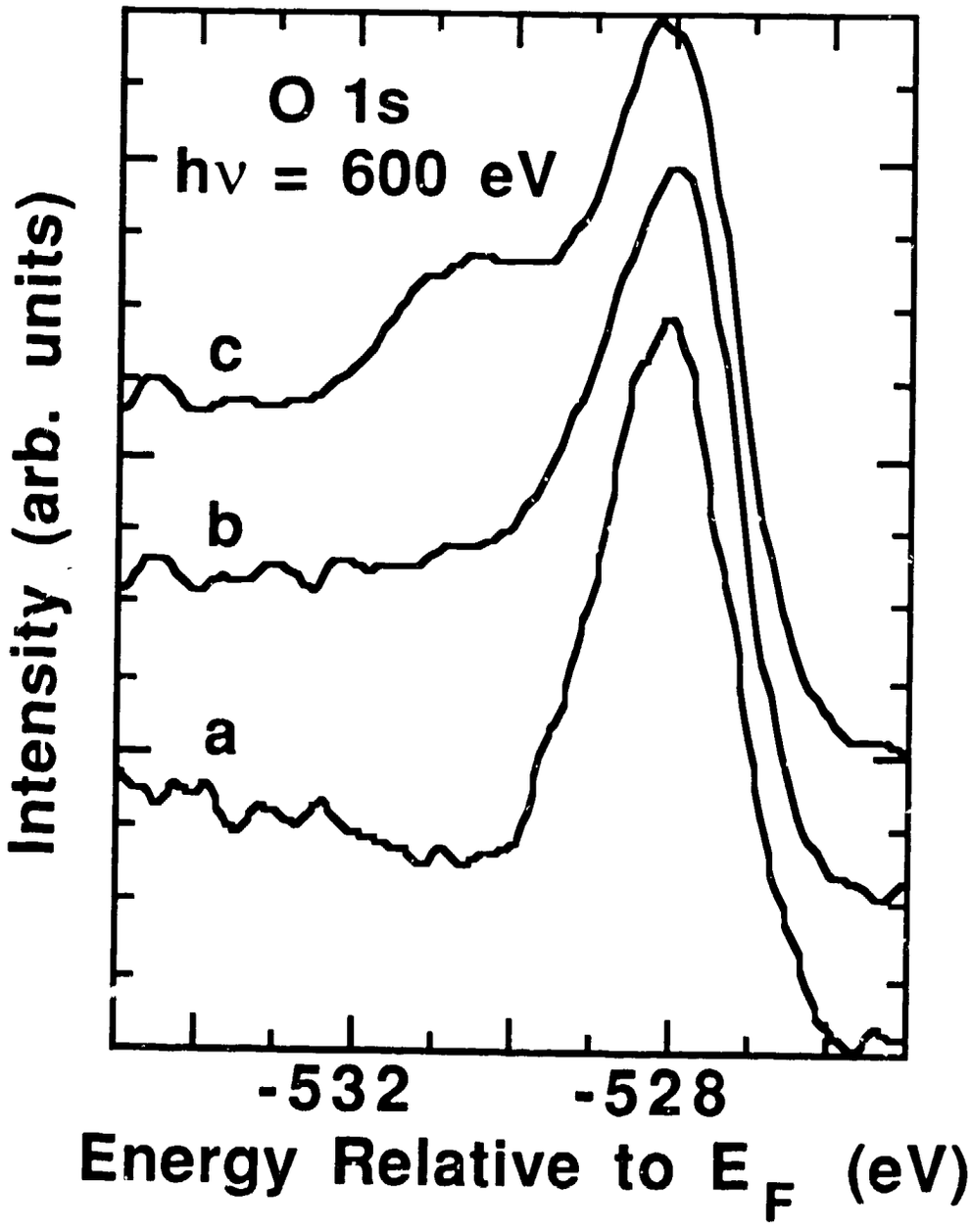
O 1s
hν = 600 eV
c
b
a
Intensity (arb. units)
-532
-528
Energy Relative to E_F (eV)

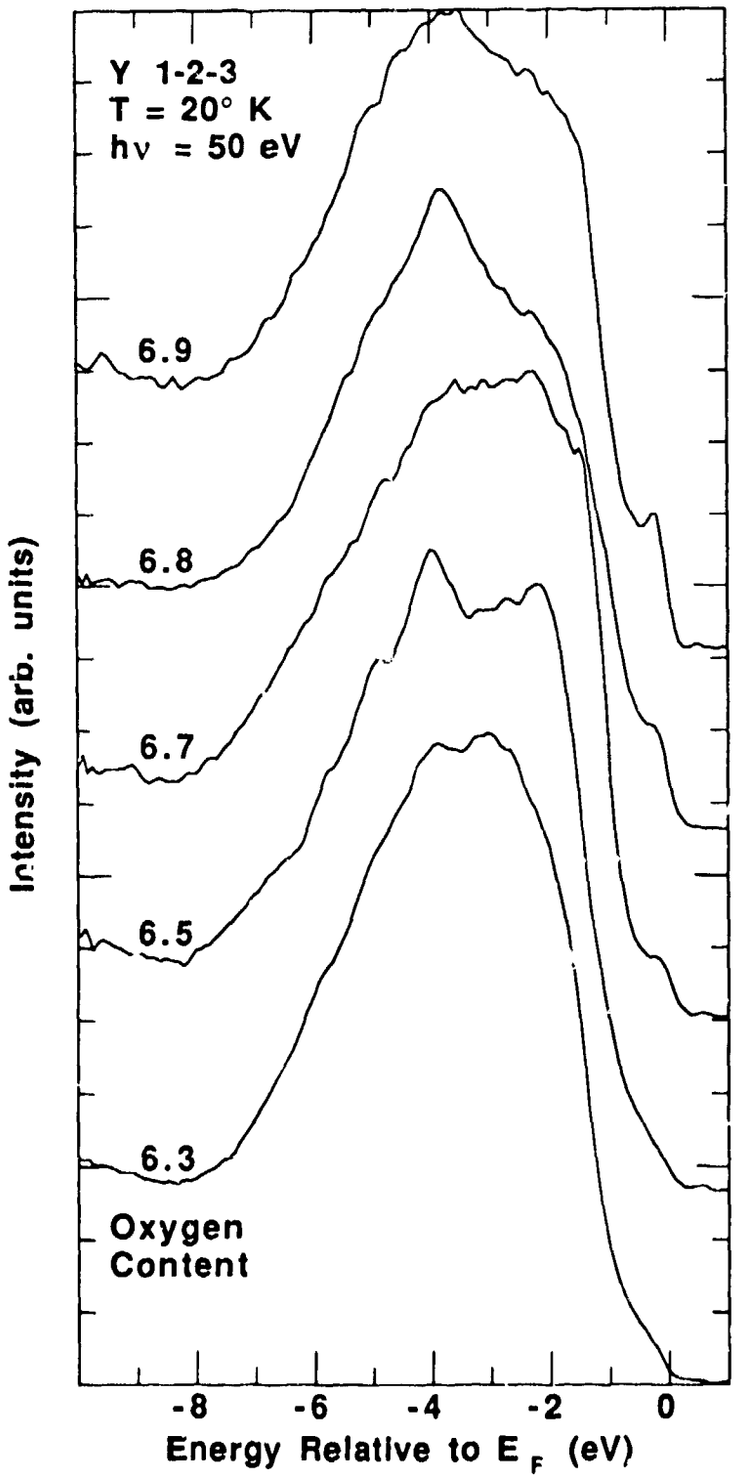
Y 1-2-3
T = 20° K
hν = 50 eV
6.9
6.8
6.7
6.5
6.3
Oxygen
Content
Intensity (arb. units)
-8
-6
-4
-2
0
Energy Relative to E F (eV)

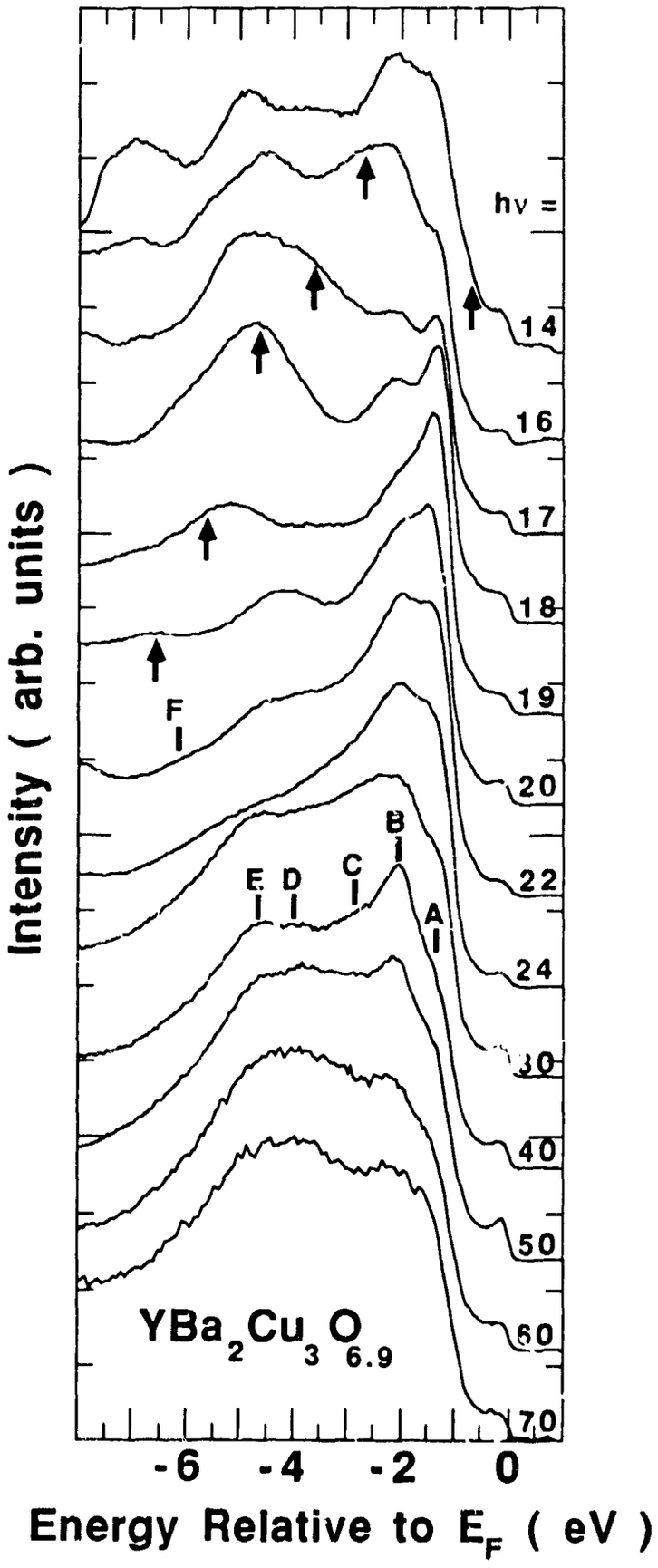
hν =
14
16
17
18
19
20
22
24
30
40
50
60
70
F
E
D
C
B
A
YBa2Cu3O6.9
-6
-4
-2
0
Intensity (arb. units)
Energy Relative to E_F (eV)

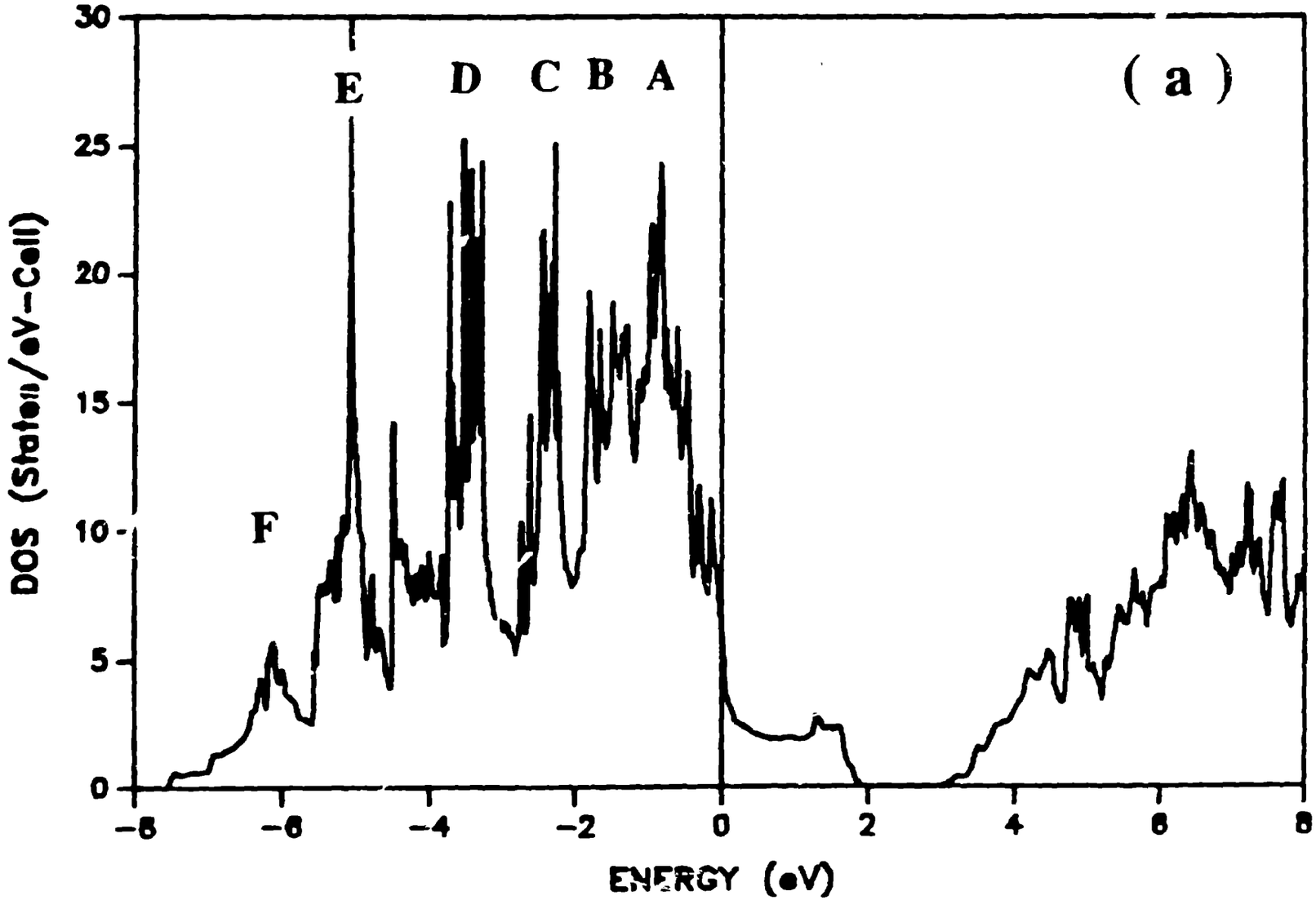
30
25
20
15
10
5
0
DOS (States/eV-Cell)
E
D
C
B
A
F
(a)
−8
−6
−4
−2
0
2
4
6
8
ENERGY (eV)

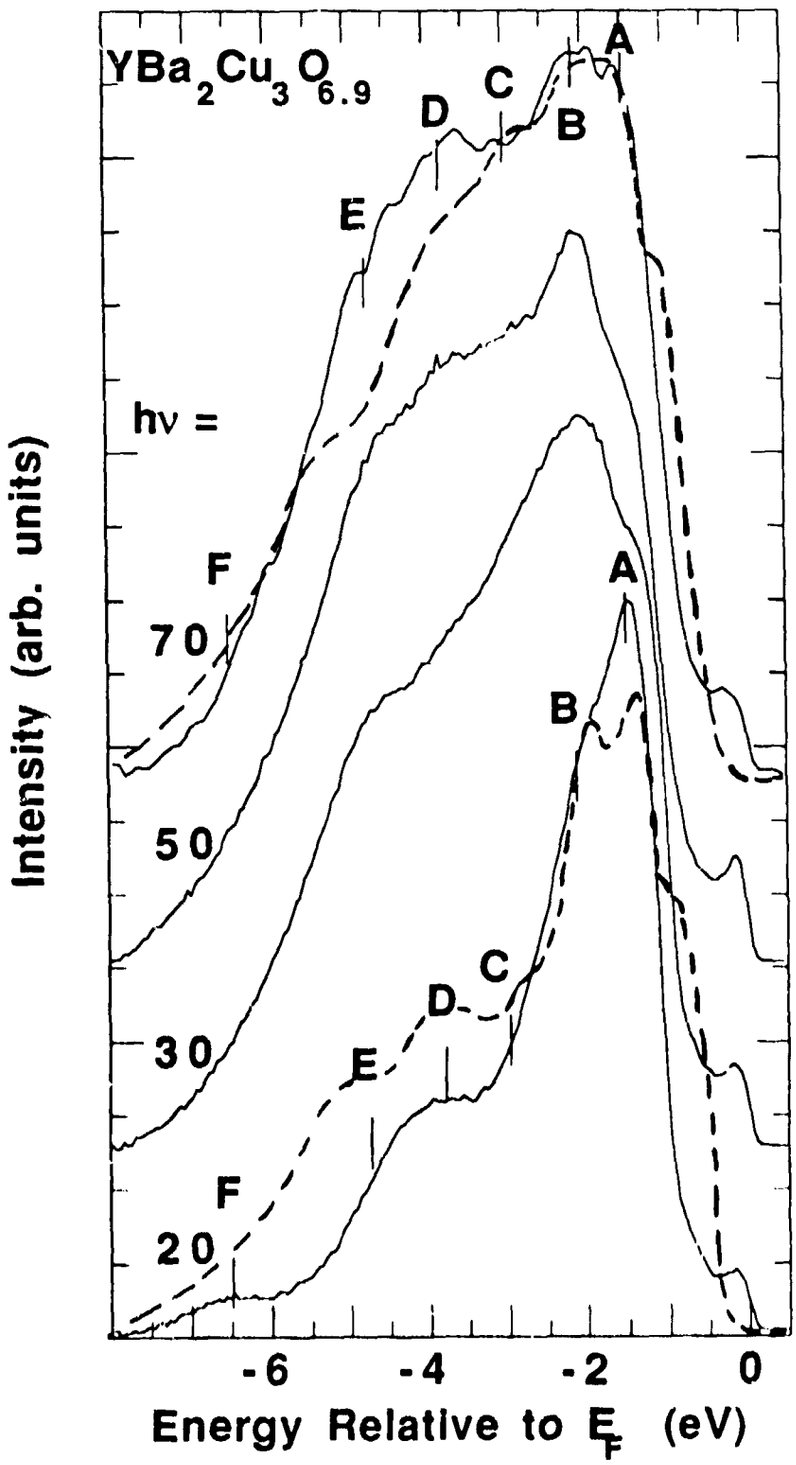
YBa2Cu3O6.9
A
B
C
D
E
F
hν =
70
50
30
20
A
B
C
D
E
F
Intensity (arb. units)
-6
-4
-2
0
Energy Relative to E_F (eV)

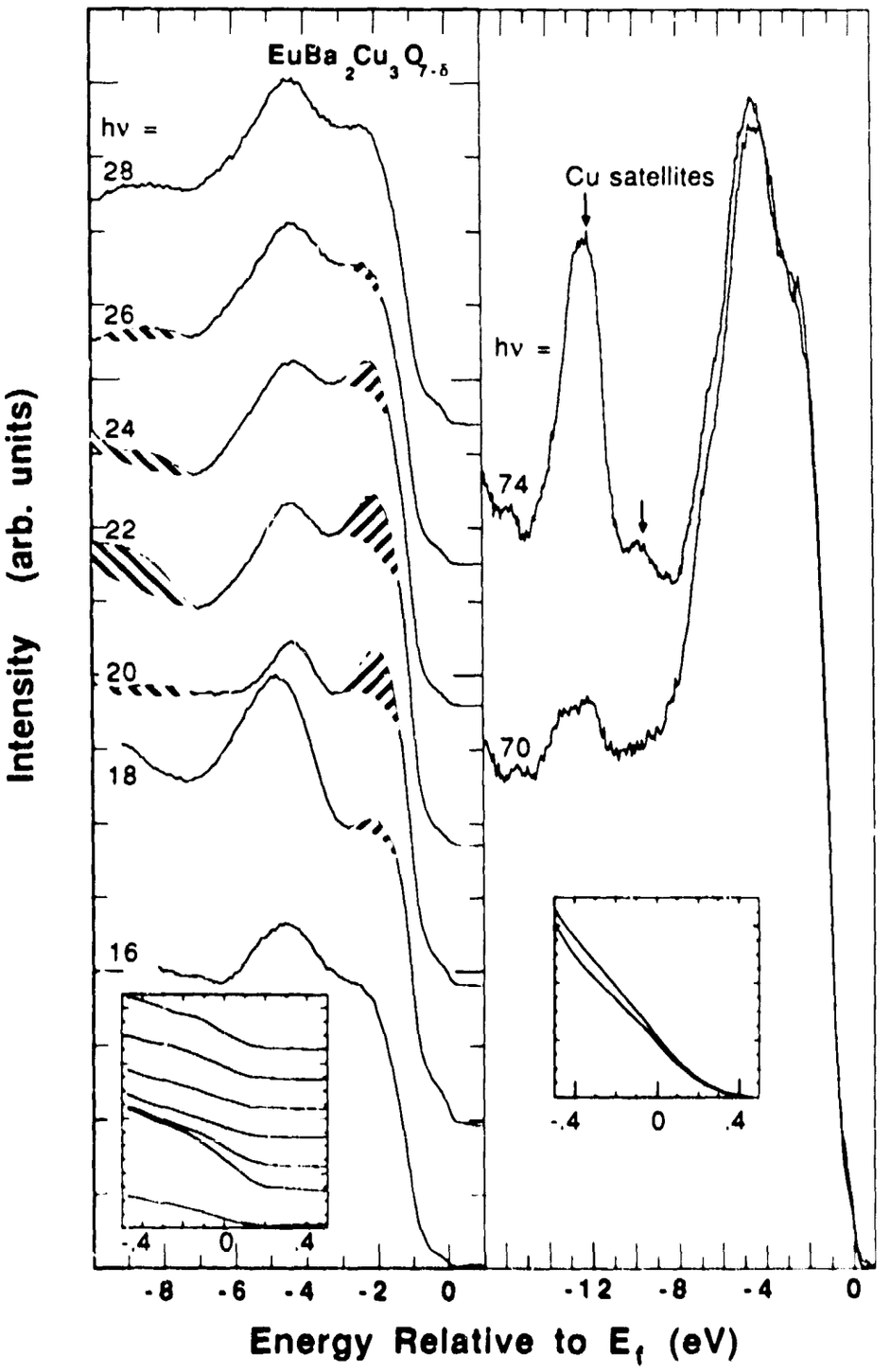
EuBa2Cu3O7-δ
hν =
28
26
24
22
20
18
16
Cu satellites
hν =
74
70
-.4
0
.4
-8
-6
-4
-2
0
-12
-8
-4
0
Intensity (arb. units)
Energy Relative to E_f (eV)

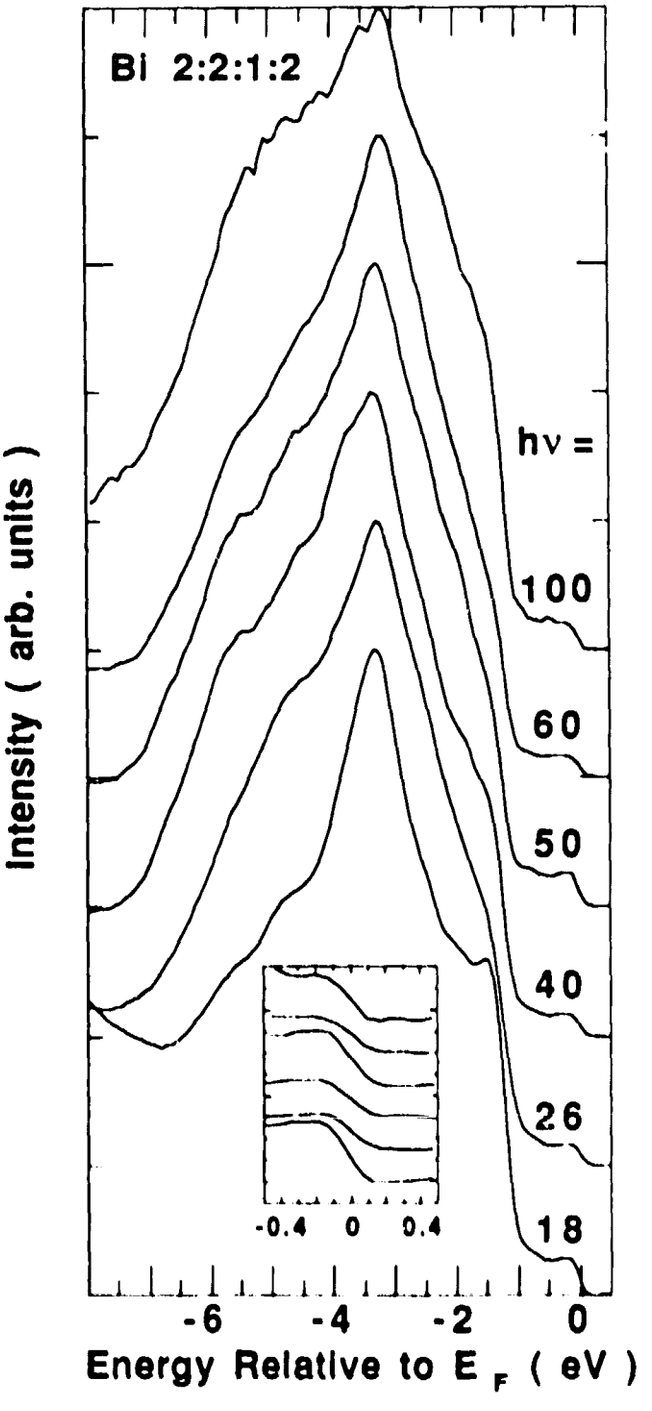
Bi 2:2:1:2
hν =
100
60
50
40
26
18
-0.4
0
0.4
-6
-4
-2
0
Energy Relative to E F (eV)
Intensity (arb. units)

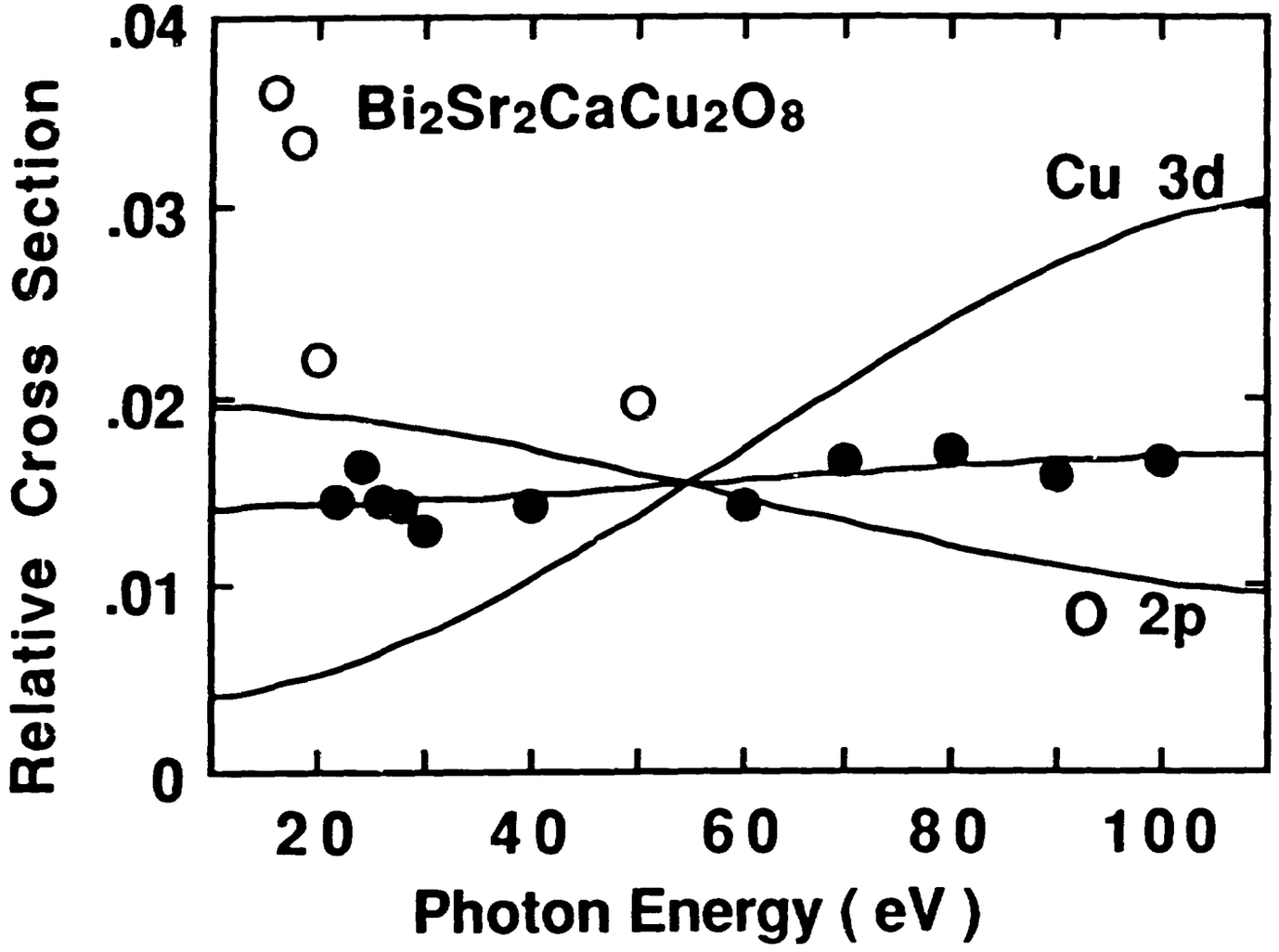
.04
.03
.02
.01
0
Relative Cross Section
Bi2Sr2CaCu2O8
Cu 3d
O 2p
20
40
60
80
100
Photon Energy (eV)

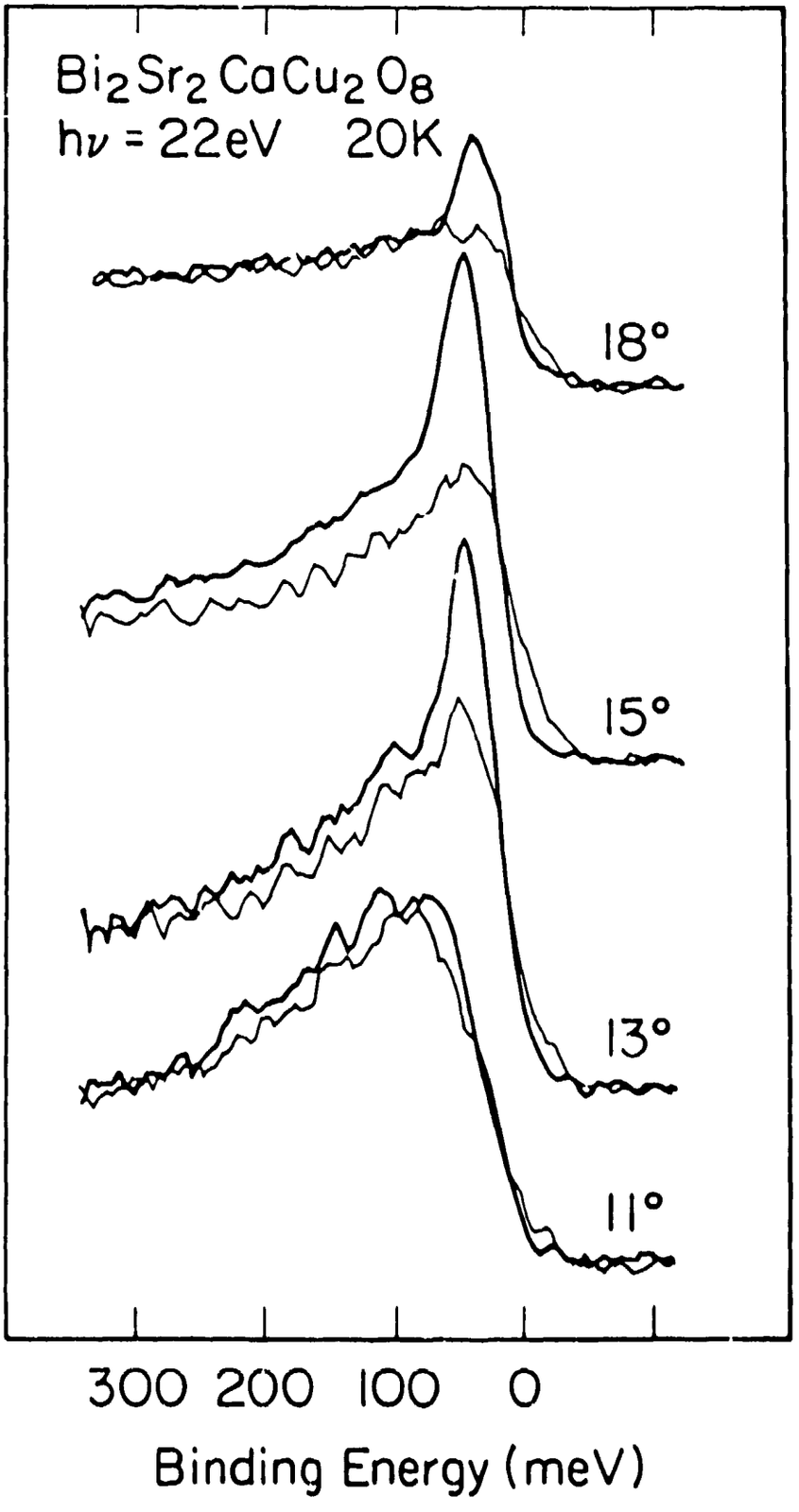
$Bi_2Sr_2CaCu_2O_8$
$h\nu$ = 22eV 20K
18°
15°
13°
11°
300 200 100 0
Binding Energy (meV)

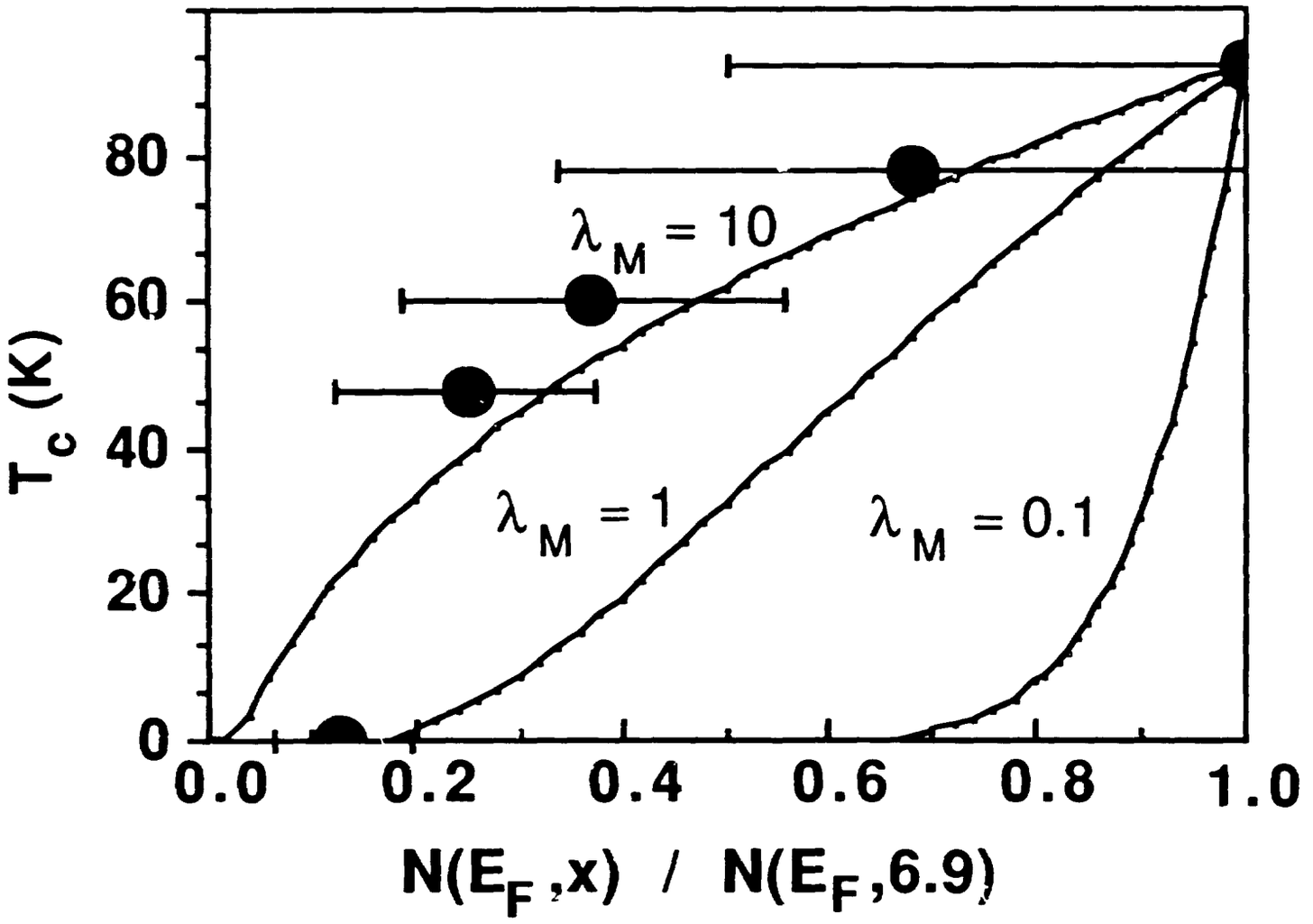
80
60
40
20
0
T_c (K)
$\lambda_M = 10$
$\lambda_M = 1$
$\lambda_M = 0.1$
0.0
0.2
0.4
0.6
0.8
1.0
$N(E_F,x)$ / $N(E_F,6.9)$